J. Opt. A: Pure Appl. Opt. **8** (2006) S550–S553 doi:10.1088/1464-4258/8/7/S39

# Focused ion beam fabrication of one-dimensional photonic crystals on $Si_3N_4/SiO_2$ channel waveguides

**S Cabrini[1], L Businaro[1], M Prasciolu[1], A Carpentiro[1], D Gerace[2], M Galli[2], L C Andreani[2], F Riboli[3], L Pavesi[3] and E Di Fabrizio[4]**

[1] TASC CNR-INFM, Area Science Park, S.S.14 km 163.5, 34012 Basovizza, Trieste, Italy
[2] Dipartimento di Fisica 'A Volta', Università di Pavia, via Bassi 6, 27100 Pavia, Italy
[3] Dipartimento di Fisica, Università di Trento, via Sommarive 14, I-38050 Povo (Trento), Italy
[4] Università della Magna Graecia, viale Europa, Campus Germaneto–88100-Catanzaro, Italy

Received 3 January 2006, accepted for publication 10 April 2006
Published 12 June 2006
Online at stacks.iop.org/JOptA/8/S550

**Abstract**
In this paper we describe a reliable and expedient approach for protyping one-dimensional (1D) photonic crystal (PhC) on optical waveguides using focused ion beam (FIB) lithography (which eliminates the need for photoresist and alignment markers). In particular, we show the detailed fabrication process of three 1D photonic crystal patterns (1) a periodic structure, (2) with micrometre-wide cavity layers, and (3) with one taper element, directly milled onto a silicon nitride/silicon dioxide ($Si_3N_4/SiO_2$) channel waveguide. Experimental investigations of the devices obtained using ultra-broadband transmittance spectroscopy in the visible and near-infrared frequency ranges (i.e. wavelengths between 0.4 and 1.7 $\mu$m) are employed to show photonic band-gap behaviour up to fourth order in the radiative mode region. These results are compared with simulations of both transmission and photonic dispersion behaviour. In addition, we demonstrate the novel effects produced by taper elements on the 1D PhC micro-cavities.

**Keywords:** focused ion beam lithography, photonic crystals, optical waveguide, photonic band-gap

(Some figures in this article are in colour only in the electronic version)

## 1. Introduction

Silicon-based photonics is an ideal method for manipulating, controlling, and detecting light at sub-micrometre length scales [1]. The high index contrast between silicon-based materials and air, which spans from 1 for $Si_3N_4$ up to 2.5 for Si, makes these systems ideal for devices associated with photonic band-gap materials. Among these are electromagnetic resonant cavities, which are able to trap light and are considered to be building blocks of future photonic circuits [2]. In these systems, photon confinement within a finite volume is assured by periodic refractive index modulation of the surrounding medium.

Periodic microstructures deeply etched into a semiconductor waveguide offer high refractive-index contrasts and much shorter interaction lengths with respect to many other materials. Examples include photonic wires or air-bridge micro-cavities [3, 4]. Responding to the quest for miniaturization in optoelectronics, very compact Bragg reflectors [5, 6] can be implemented in short cavities, offering opportunities to use large free spectral ranges, small modal volumes (required for controlling the spontaneous emission of atoms in the cavity), and low threshold lasers. Most implementations have been patterned using electron beam lithography (EBL) followed by carefully optimized reactive ion etching processes (RIE) [7]. Focused ion beam (FIB) milling is an alternative and rapid prototyping technique used in order to verify the effectiveness of the 1D and 2D PhC geometry. With FIB lithography, patterns are transferred by direct impingement of the ion beam on the substrate [8, 9] which allows the rapid fabrication of several prototype devices without the need for a resist, etching mask, or complicated etching recipe development. Further-

© 2006 IOP Publishing Ltd Printed in the UK

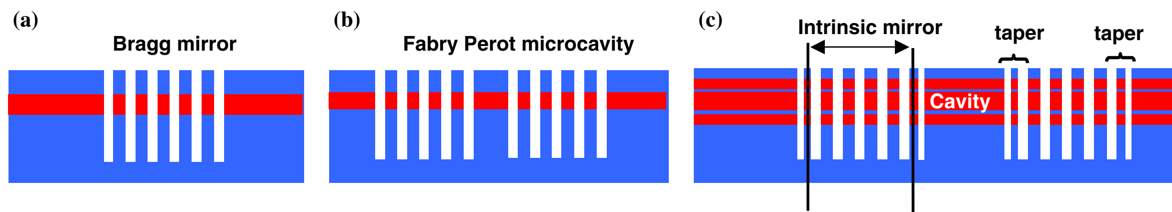


**Figure 1.** Schemes of the three 1D PhCs fabricated: (a) single Bragg mirror; (b) Fabry–Perot micro-cavity; and (c) micro-cavity with optimized mirror (taper elements). The lattice constant is $a = 525$ nm.

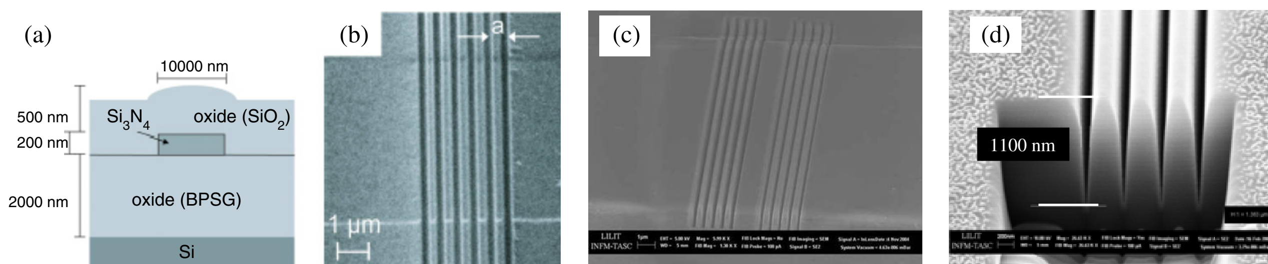


**Figure 2.** (a) Schematic illustration of the $Si_3N_4$ channel waveguide. (b) Top view of the waveguide-embedded Bragg mirror with six air slits (FIB image): the lattice constant is $a = 525$ nm. (c) SEM image of the sample with a cavity layer between Bragg mirrors with five air slits per side. (d) SEM image of a cross section of the final structure.

more, this technique can be applied to a wide range of applications where other techniques, such as EBL, are prohibitive. For example, with FIB lithography, we can directly process highly non-planar samples. In FIB, direct milling technology, operating the FIB with an appropriate beam size, shape, current and energy to remove the required amount of material from a pre-defined location in a controllable manner, is crucial. Here we employ a CrossBeam LEO XB1540, which combines a 30 keV gallium ion beam column with a 30 keV electron beam GEMINI column. Using this system, we take advantage of all the features that a FIB lithography offers, and in addition we have the opportunity to easily and accurately align the PhC pattern to a pre-patterned optical waveguide; there is no need to use alignment markers or to implement a sophisticated alignment procedure.

Herein, we present the fabrication of 1D PhC structures on optical waveguides for use as standard Bragg mirrors, with a cavity and tapered by means of an FIB process. In addition, the optical characterization of the devices is presented.

## 2. 1D photonic crystals

A 1D PhC slab is the waveguide-embedded analogue of the well-known Bragg mirror. Together with PhC slab resonators, i.e. the analogue of Fabry–Perot cavities, they represent key elements for future PhC-based integrated circuits.

The 1D refractive index modulation is achieved by producing air trenches across the channel waveguide. A 1D photonic crystal with a defect is also described as a Fabry–Perot microcavity. This is formed by two first-order Bragg mirrors separated by a spacer. The Bragg mirrors consist of a sequence of $\lambda/2$-thick periods, where each period contains an air slit and a waveguide segment (where $\lambda$ is an optical thickness). An optical mode propagating in the channel waveguide excites many cavity radiative modes when it is transmitted through the cavity. This fact degrades the quality factor ($Q$-factor) of the cavity. Indeed, the key point for high $Q$-factor cavities relies on fine tuning of the first periods facing the cavity spacer [10–12] to reduce the excitation of radiative cavity modes and thus decrease the impedance mismatch between the waveguide and cavity modes. In figure 1, the schemes of the three 1D PhCs fabricated are shown: (a) a single Bragg mirror; (b) a Fabry–Perot (FP) micro-cavity; and (c) a micro-cavity with an optimized mirror [13, 14].

## 3. Fabrication process

Low-loss $Si_3N_4/SiO_2$ channel waveguides are produced within a complementary metal-oxide semiconductor (CMOS) fabrication pilot-line by low-pressure chemical vapour deposition (LPCVD). Employing LPCVD reduces the interface roughness and, as a consequence, the scattering losses. A 2.0 $\mu$m cladding layer of boron-phosphor-silicate glass (BPSG) is deposited on a 4 inch Si wafer. Then, a 200 nm-thick $Si_3N_4$ guiding layer is deposited by an LPCVD process and 2D rib waveguides with a 10 $\mu$m-wide rectangular cross-section are defined by lithography and etching. Channel waveguides are obtained by covering the $Si_3N_4$ rib with a 500 nm-thick layer of a medium-temperature LPCVD tetraethyl orthosilicate $SiO_2$ top cladding. The scheme of the channel waveguide used for successive 1D patterning is seen in figure 2(a). The material refractive index is slightly dispersive around the values $n(Si_3N_4) = 2$ and $n(SiO_2) \sim n(BPSG) = 1.45$ at a wavelength $\lambda = 1.5$ $\mu$m [13].

In our experiment, we used the LEO-ZEISS 1540XB CrossBeam, comprising a high-resolution 30 keV Ga+ FIB column to mill directly in combination with a high-precision field emission gun (FEG) scanning electron microscope (SEM) for precise positioning and inspection of the fabricated nanostructures in real time. Using an ion current of about

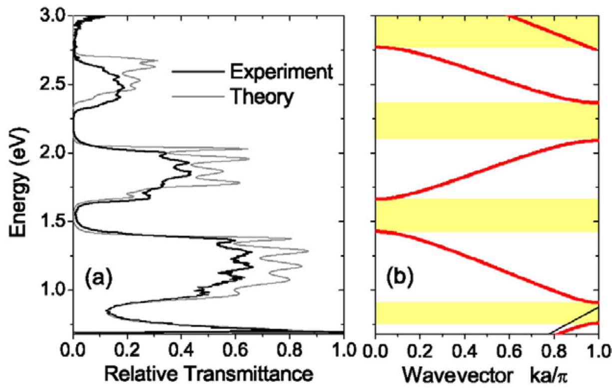


**Figure 3.** (a) The relative transmittance for the waveguide-embedded Bragg mirror relative to figures 1(a) and 2(b). (b) Photonic band dispersion of the 1D PhC slab. Photonic band-gaps of the fundamental mode are highlighted.

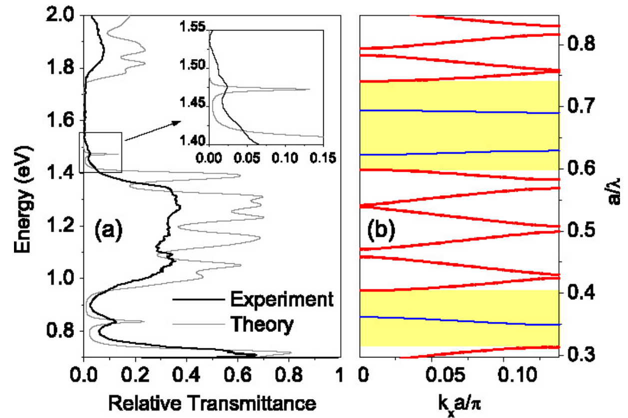


**Figure 4.** (a) The relative transmittance for the waveguide-embedded microcavity of figures 1(b) and 2(c). (b) Photonic band dispersion of a 1D PhC slab with a supercell in the plane. The band-gap regions are highlighted.

100 pA and controlling the FIB with a pattern generator (RAITH ELPHY), the pattern is directly written onto the sample surface. Using a total ion dose of 660 mA s cm$^{-2}$, a depth of about 1 $\mu$m for each structure can be obtained. Figures 2(b) and (c) show a scanning ion microscope image (FIB image) and an SEM image of a fabricated samples.

In order to obtain approximately 1 $\mu$m-deep and 100 nm-wide structures (10:1 aspect ratio), a special milling strategy was performed. Here we performed multiple passes on each line with 0.69 mAs cm$^{-2}$, nominally 80 nm wide, repeated 32 times before passing to the next line. The entire pattern was repeated in 30 identical loops. This takes a total of 30–40 min for the final device. Compared with achieving this structure in a single pass, the multiple-pass method uses a smaller dose for each structure that increases the efficiency of the milling process due to the small amount of sputtered materials re-deposited on the side walls and the small amount of heating of the substrate. The cross section of the final cut is shown in figure 2(d). The depth is more than 1 $\mu$m, indicating a quasi-symmetrical guide, but the cut has a V shape instead of a U shape. However, in the proximity of the optical guide, the two walls are approximately parallel. Furthermore, the surface is smooth and regular.

## 4. Optical characterization

Transmission measurements are performed with an end-fire coupling scheme. The broadband light emitted from a mercury lamp is first sent to a Fourier-transform spectrometer (Bruker IFS 66 s) for spectral analysis [14]. The beam is then brought to the set-up via a fiber and focused on the sample facet by means of a 25× reflecting microscope objective. A second identical objective is used to collect the light at the exit of the other waveguide facet and to re-focus it onto the detector. An infrared vidicon camera allows viewing of both facets of the sample for proper alignment of the waveguide on the optical axis of the measuring system. Spectra are taken in the 0.73–3 eV energy range (1.7–0.4 $\mu$m wavelength range) by means of Si and InGaAs PiN photodiodes. Light polarization is selected by means of a calcite Glan–Taylor polarizer. The spectral range on the low-energy side is limited by the response of the InGaAs photodiode. Transmission through the samples is normalized to a reference channel waveguide without patterned regions.

The relative transmittance for the waveguide-embedded Bragg mirror (figures 1(a) and (b)) is shown in figure 3. Transverse-electric (TE) polarized light is selected at the input facet. The measured spectrum shows the defined stop-bands up to the fourth order very well, which increase in spectral width by increasing the energy. The relative transmission intensity in the regions outside the stop bands is rather high, around 70% at low energy, while it decreases rapidly to below 20% for photon energies above 2.5 eV in the visible region. Fabry–Perot oscillations (corresponding to the Bloch-mode interference of the 1D system) are also clearly resolved in the transmitting regions. The spectra are compared to transmission calculations performed with an eigenmode expansion-based solver (FIMMWAVE, commercial software). Eigenmode expansion belongs to the class of scattering matrix methods, which provide an exact solution of Maxwell's equations in the frequency domain system.

In figure 4, experimental results are shown for the waveguide-embedded microcavity of figures 1(b) and 2(c). Good agreement between measured and calculated TE transmittance spectra is found. A resonant cavity mode with an energy of 0.835 eV ($\lambda = 1.485$ $\mu$m) and a measured $Q$-factor of about 22 is clearly visible within the fundamental photonic band-gap. A second cavity mode is excited at an energy of 1.475 eV ($\lambda = 0.84$ $\mu$m) within the second-order band-gap (see the inset of figure 4), with a much lower $Q$-factor owing to the enhanced intrinsic losses and to the amplification of disorder-induced losses at shorter wavelengths.

Figure 5 shows the relative transmittance of TE-polarized light for the engineered FP micro-cavity of figure 1(c). The measured spectrum shows a well-defined band-edge at 1380 nm and the resonant peak at 1515 nm. The first FP oscillation can be observed between 1300 and 1380 nm. The measured full width at half maximum (FWHM) of the resonance peak is 15 nm, which corresponds to a quality factor of $Q = 105$. The spectrum is compared with the numerical calculation (the line in figure 5) and a reasonably good fit is found for the spectral position of the FP stop-band, the resonance position and width, while the baseline

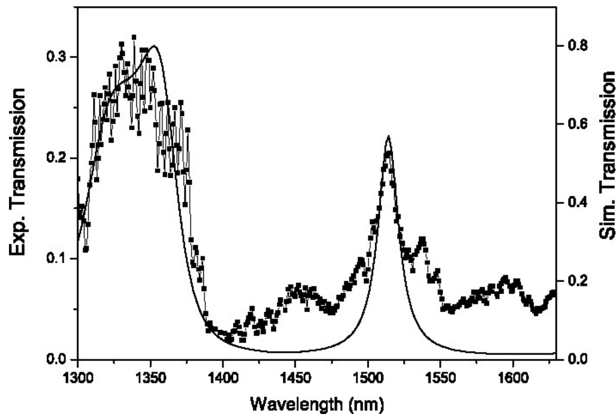


**Figure 5.** Transmittance of TE-polarized light for the engineered FP microcavity of figure 1(c).

in the photonic band-gap region is not reproduced due to diffraction losses and light leakage not taken into account in the calculations. The Q-factor calculated using the classical FP model is twice as large as the measured one. Figure 6 shows a fabricated microcavity with one taper element on the optical waveguide.

## 5. Discussion

Figures 3–5 show relatively good agreement between the simulated and actual measurements on the devices. The expected decrease in transmission intensity with increasing energies is present. Small differences in frequency response and $Q$ values for the devices are present and can be attributed to diffraction losses caused by surface and bulk disorder and to the non-uniform width/depth ratio in the FIB devices. For the Bragg reflector (figure 3), this is most evident for energies higher than 2.2 eV, where the propagation is more sensitive to these non-uniformities. For the FP device (figure 4), it shows up at lower energies because the FP is channeling the light through a cavity and thus the non-uniformity effects are amplified.

Although we have realized prototype photonic device fabrication in a novel and efficient way using FIB lithography, our future efforts will be directed to controlling the surface and bulk non-uniformities and the exact shape of the cavity.

## 6. Conclusions

We have shown that the FIB lithographic process is a very powerful and versatile technique for the prototyping of new photonic devices and for the *in situ* modification of pre-patterned ones. 1D PhC slabs in $Si_3N_4/SiO_2$ waveguides have been fabricated successfully using FIB lithography on a thin film embedded on a bulk substrate. Characterization was performed by means of wide-band transmission spectroscopy in the near-infrared and visible ranges. The reliability of the photonic band-gap concept in the quasi-guided mode region and the existence of cavity modes within the band-gap for structures containing defect layers have been shown.

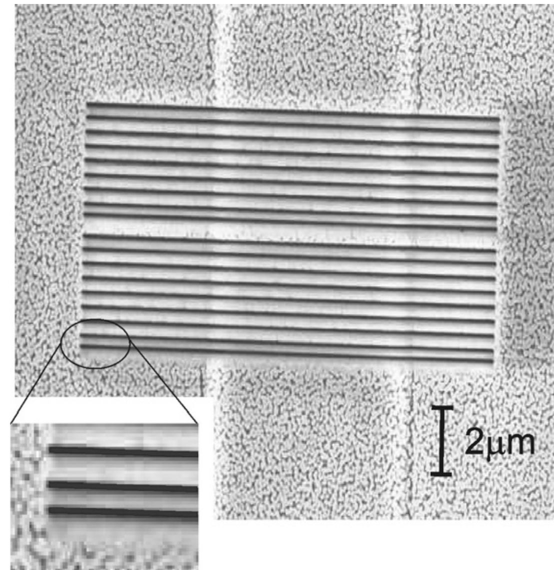


**Figure 6.** SEM image of the tapered cavity on the optical waveguide with detail of the taper element of the grating.

These results are important for the realization of silicon-based photonic integrated circuits.

## Acknowledgments

This work was supported by Ministero dell'Istruzione, dell'Università e della Ricerca (MIUR) through the Cofin Program 'Silicon-based photonic crystals'.

## References

[1] Pavesi L and Lockwood D (ed) 2004 *Silicon Photonics* (*Springer Topics in Applied Physics* vol 94) (Berlin: Springer)
[2] Vahala K J 2003 *Nature* **424** 839–46
[3] Zhang J P, Chu D Y, Wu S L, Bi W G, Tiberio R C, Joseph R M, Taflove A, Tu C W and Ho S T 1996 *IEEE Photon. Technol. Lett.* **8** 491
[4] Foresi J S, Villeneuve P R, Ferrera J, Thoen E R, Steinmeyer G, Fan S, Joannopoulos J D, Kimerling L C, Smith H I and Ippen E P 1997 *Nature* **390** 143
[5] Krauss T F and De La Rue R M 1996 *Appl. Phys. Lett.* **68** 1613
[6] Baba T, Hamasaki M, Watanabe N, Kaewplung P, Matsutani A, Mukaihara T, Koyama F and Iga K 1996 *Japan. J. Appl. Phys.* 1 **35** 1390
[7] Peyrade D, Silberstein E, Lalanne Ph, Talneau A and Chen Y 2002 *Appl. Phys. Lett.* **81** (5)
[8] Valiev K A 1992 *The Physics of Sub-micron Lithography* (New York: Plenum)
[9] Cabrini S *et al* 2005 *Microelectron. Eng.* **78/79** 11
[10] Song B S, Noda S, Asano T and Akahane Y 2005 *Nat. Mater.* **4** 207
[11] Johnson S G, Fan S, Mekis A and Joannopoulos J D 2001 *Appl. Phys. Lett.* **78** 3388
[12] Lalanne P and Hugonin J P 2003 *IEEE J. Quantum Electron.* **39** 1430–8
[13] Gerace D *et al* 2005 *Appl. Phys. Lett.* **87** 211116
[14] Riboli F, Recati A, Daldosso N, Pavesi L, Pucker G, Lui A, Cabrini S and Di Fabrizio E 2006 *Photon. Nanostruct. Fundam. Appl.* **4** 41–6